Journal of Alloys and Compounds 689 (2016) 726–732

Contents lists available at ScienceDirect

Journal of Alloys and Compounds

journal homepage: http://www.elsevier.com/locate/jalcom

Ab-initio, Mößbauer spectroscopy, and magnetic study of the approximant $Al_{72}Ni_9Fe_{19}$ to a decagonal Al-Ni-Fe quasicrystal

Farshad Nejadsattari [a], Zbigniew M. Stadnik [a, *], Janusz Przewoźnik [b], Benjamin Grushko [c]

[a] Department of Physics, University of Ottawa, Ottawa, Ontario, K1N 6N5, Canada
[b] Solid State Physics Department, Faculty of Physics and Applied Computer Science, AGH University of Science and Technology, 30-059, Kraków, Poland
[c] PGI-5 Forschungszentrum Jülich, D-52425, Jülich, Germany

ARTICLE INFO

Article history:
Received 18 May 2016
Received in revised form
2 August 2016
Accepted 3 August 2016
Available online 6 August 2016

Keywords:
Paramagnet
^{57}Fe Mößbauer spectroscopy
Electric quadrupole splitting
Pseudogap in the density of states
Debye temperature

ABSTRACT

We report the results of *ab-initio* electronic structure and electric field gradient calculations and of X-ray diffraction, ^{57}Fe Mößbauer spectroscopy, and magnetic studies of the approximant $Al_{72}Ni_9Fe_{19}$ to a decagonal Al-Ni-Fe quasicrystal. The approximant crystallizes in the hexagonal space group $P6_3/mmc$ with the lattice parameters $a = 7.6989(2)$ Å and $c = 7.6724(2)$ Å. A pseudogap in the density of states, centered at ~0.30 eV above the Fermi level and with a width of ~0.35 eV, is found. Evidence for the covalent nature of the chemical bonding and good metallicity of $Al_{72}Ni_9Fe_{19}$ is provided. The Mößbauer spectra and a $1/T$-like dependence of the magnetic susceptibility indicate that $Al_{72}Ni_9Fe_{19}$ is a paramagnet down to 2.0 K. The shape of the Mößbauer spectra is accounted for by a superposition of two quadrupole doublets corresponding to Fe atoms located at two inequivalent crystallographic sites. A sudden change of the quadrupole splittings of the two doublets at ~200 K indicates a possible structural phase transition. Excellent agreement between the calculated and measured quadrupole splittings is observed. The Debye temperature of $Al_{72}Ni_9Fe_{19}$ is found to be 431 (3) K.

1. Introduction

Solids are formed as crystalline, quasicrystalline, or amorphous. Quasicrystals (quasicrystalline solids) possess a new type of long-range translational order, quasiperiodicity, and a noncrystallographic orientational order associated with classically forbidden fivefold, eightfold, tenfold, and twelvefold symmetry axes [1]. Discovery of new quasicrystals [2] and studies of their physical properties [3] are often helped by studying so-called approximants. An approximant to a quasicrystal is a structurally complex crystalline compound whose composition and structural units are very similar to those of the quasicrystal [4–6].

The intermetallic compound Al_5Co_2 was shown [7] to be an approximant to Al-Co-based decagonal quasicrystals. The first refinement of the Al_5Co_2 crystal structure, that was based on the analysis of the diffraction intensities obtained from Weisenberg photographs of single crystals [8], established that Al_5Co_2 crystallizes in the hexagonal space group $P6_3/mmc$ with the lattice parameters $a = 7.656(3)$ Å and $c = 7.593(2)$ Å. Other refinements that followed, of both powder and single crystal X-ray diffraction data of Al_5Co_2 [9,10], confirmed the correctness of the choice of the space group.

Electronic structure calculations predict [11–14] the presence of a minimum in the Al_5Co_2 density of states (DOS), called a pseudogap, at the Fermi energy (E_F). The existence of such a pseudogap at or in the close vicinity of E_F is a characteristic DOS feature of some decagonal and all icosahedral quasicrystals [1]. The existence of the theoretically predicted pseudogap in the DOS(E_F) of Al_5Co_2 was confirmed experimentally [12].

It was Bradley and Taylor [15] who observed for the first time that the structure of ternary Al-rich Al-Ni-Fe alloys containing Fe and Ni in certain proportions is the same as that of Al_5Co_2. Specifically, they found out that $Al_{10}NiFe_3$ ($Al_{71.4}Ni_{7.1}Fe_{21.4}$) has exactly the same type of structure as Al_5Co_2, but did not provide the lattice parameters of the hexagonal unit cell of $Al_{10}NiFe_3$. Thus, $Al_{10}NiFe_3$ can be regarded as an approximant to a decagonal Al-Ni-Fe quasicrystal. The lattice parameters $a = 7.70937(5)$ Å and $c = 7.67947(8)$ Å and atomic coordinates for an alloy of similar nominal composition $Al_{71.5}Ni_{10}Fe_{18.5}$ (empirical composition $Al_{71.4}Ni_{10.2}Fe_{19.1}$) were determined from the single crystal X-ray diffraction data [16].

* Corresponding author.
E-mail address: stadnik@uottawa.ca (Z.M. Stadnik).

http://dx.doi.org/10.1016/j.jallcom.2016.08.021
0925-8388/

Here we report the results of *ab-initio*, X-ray diffraction, ^{57}Fe Mößbauer spectroscopy, and magnetic study of $Al_{72}Ni_9Fe_{19}$, an approximant to a decagonal Al-Ni-Fe quasicrystal.

2. Theoretical and experimental methods

Ab initio electronic structure and Mößbauer hyperfine-interaction parameter calculations have been performed within the framework of density functional theory using the full-potential linearized augmented-plane-wave plus local orbitals (FP-LAPW+lo) method as implemented in the WIEN2k package [17]. In this method, the unit cell is partitioned into two regions: a region of non-overlapping muffin-tin (MT) spheres centered at the atomic sites and an interstitial region. The wave functions in the MT regions are a linear combination of atomic radial functions times spherical harmonics, whereas in the interstitial regions they are expanded in plane waves. The basis set inside each MT sphere is split into a core and a valence subset. The core states are treated within the spherical part of the potential only and are assumed to have a spherically symmetric charge density in the MT spheres. The valence wave functions in the interstitial region were expanded in spherical harmonics up to $l = 4$, whereas in the MT region they were expanded to a maximum of $l = 12$ harmonics. For the exchange-correlation potential, the generalized gradient approximation (GGA) scheme of Perdew, Burke, and Ernzerhof [18] was used. A separation energy of −6.0 Ry between the valence and core states of individual atoms in the unit cell was chosen.

The values of 1.99, 2.31, and 2.31 a.u. were used as the MT radii for Al, Fe, and Ni, respectively. The plane-wave cut-off parameter was set to $R_{MT} \times K_{MAX} = 6.5$, where R_{MT} is the smallest MT radius in the unit cell and K_{MAX} is the maximum K vector used in the plane-wave expansion in the interstitial region. A total of 1000 k-points were used within a $10 \times 10 \times 9$ k-mesh in the irreducible wedge of the first Brillouin zone. A convergence criterion for self-consistent field calculations was chosen in such a way that the difference in energy between two successive iterations did not exceed 10^{-4} Ry. The experimental lattice parameters (a and c) and the atomic position parameters (*vide infra*) were used in the calculations.

An ingot of nominal composition $Al_{72}Ni_9Fe_{19}$ (point 1 in Fig. 1 of [19]) was prepared by inductive melting of the constituent elements in a water-cooled copper crucible under an argon atmosphere. It was then annealed at 1073 K for 550 h and then water quenched.

X-ray diffraction measurements were carried out at 298 K in Bragg-Brentano geometry on a PANalytical X'Pert scanning diffractometer using Cu $K\alpha$ radiation in the 2θ range 20–120° in steps of 0.02°. The $K\beta$ line was eliminated by using a Kevex PSi2 Peltier-cooled solid-state Si detector.

The dc magnetization was measured in the temperature range from 2.0 to 350 K and in magnetic fields up to 90 kOe using the vibrating sample magnetometer (VSM) option of the Quantum Design physical property measurement system (PPMS). The dc magnetic susceptibility was measured using PPMS in the magnetic field of 10 kOe in the temperature range of 2–390 K.

The ^{57}Fe Mößbauer measurements [20] were conducted using a standard Mößbauer spectrometer operating in the sine mode and a ^{57}Co(Rh) source at room temperature. The spectrometer was calibrated with a 6.35-μm-thick α-Fe foil [21] and the spectra were folded. The Mößbauer absorber consisted of a mixture of powdered $Al_{72}Ni_9Fe_{19}$, and powdered boron nitride, which was pressed into a pellet and put into a high-purity, 8-μm-thick Al disk container to ensure a uniform temperature over the whole absorber. The Mößbauer absorber was put into a Mößbauer cryostat in which it was kept in a static exchange gas atmosphere at a pressure of ~6×10^{-3} mbar. The surface density of the Mößbauer absorber was 12.9 mg/cm^2. This corresponds to an effective thickness parameter $t_a = 2.3 f_a$, where f_a is the Debye-Waller factor of the absorber. Since $t_a > 1$, the resonance line shape of the Mößbauer spectra was described using a transmission integral formula [22].

3. Results and discussion

3.1. Structural characterization

The compound studied, $Al_{72}Ni_9Fe_{19}$, analogously to the Al_5Co_2 compound, crystallizes in the hexagonal space group $P6_3/mmc$ (No. 194) [8]. The crystal structure of $Al_{72}Ni_9Fe_{19}$ is shown in Fig. 1. The rods connecting the Al, Ni, and Fe atoms (Fig. 1) describe the directional covalent bonding between these atoms (*vide infra*).

Fig. 2 displays the X-ray powder diffraction pattern of $Al_{72}Ni_9Fe_{19}$. A Rietveld refinement [23] of the X-ray powder diffraction data was carried out, yielding the lattice parameters $a = 7.6989(2)$ Å and $c = 7.6724(2)$ Å, and the atomic positional parameters that are listed in Table 1. The values of these lattice and atomic positional parameters are very close to the corresponding values for the $Al_{71.5}Ni_{10}Fe_{18.5}$ alloy [16]. No second phase/phases could be detected in the X-ray diffraction pattern of $Al_{72}Ni_9Fe_{19}$ (Fig. 2).

3.2. Ab-initio calculations

3.2.1. Electronic structure

The calculated total and atom-resolved density of states (DOS) of $Al_{72}Ni_9Fe_{19}$ is shown in Fig. 3. One observes that the total DOS outside the energy region from about −4 to 1 eV with respect to the

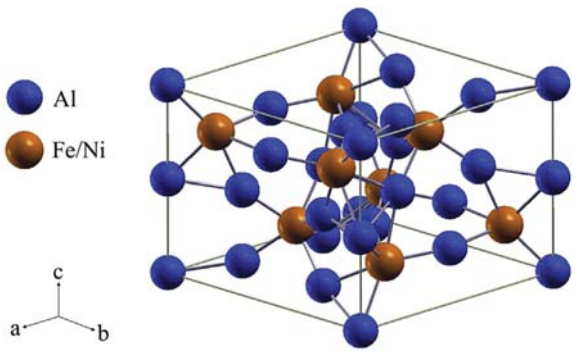

Fig. 1. The unit cell of the $Al_{72}Ni_9Fe_{19}$ compound.

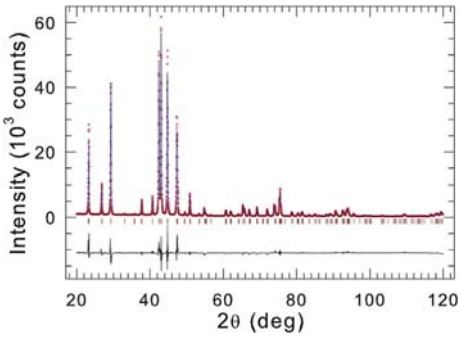

Fig. 2. Powder X-ray diffraction pattern of $Al_{72}Ni_9Fe_{19}$ at 298 K. The experimental data are denoted by open circles, while the line through the circles represents the results of the Rietveld refinement. The row of vertical bars shows the Bragg peak positions for the $P6_3/mmc$ space group. The lower solid line represents the difference curve between experimental and calculated patterns.

Table 1
Atomic positions for the hexagonal $Al_{72}Ni_9Fe_{19}$ (space group $P6_3/mmc$) obtained through Rietveld analysis and calculated V_{zz} (in units of 10^{21} V/m^2) and η.

Atom	Site	Point symmetry	x	y	z	V_{zz}	η
Al(1)	2*a*	$\bar{3}$ m	0	0	0	−2.550	0.000
Al(2)	6*h*	*mm*2	0.4647	0.9294	$\frac{1}{4}$	−4.163	0.681
Al(3)	12*k*	.*m*.	0.1935	0.3870	0.9393	−3.263	0.297
0.6786Fe(1)+0.3114Ni(1)	2*d*	$\bar{6}$ m2	$\frac{1}{3}$	$\frac{2}{3}$	$\frac{3}{4}$	−2.196	0.000
0.6786Fe(2)+0.3114Ni(2)	6*h*	*mm*2	0.1256	0.2512	$\frac{1}{4}$	−3.263	0.286

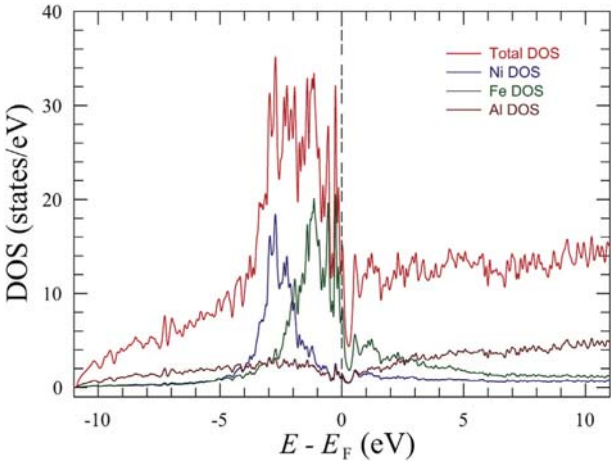

Fig. 3. Total and atom-resolved density of states of $Al_{72}Ni_9Fe_{19}$.

Fermi energy (E_F) exhibits a characteristic $E^{1/2}$ dependence predicted by the free electron model of metallic solids [24]. A similar $E^{1/2}$ dependence has been observed in other Al-rich transition metal systems [25–28]. One can understand such a DOS profile if one takes into account the fact that the Al electrons are of *s* and *p* type. The electrons in these states are weakly bound to their parent nuclei which results in a large spatial extension of their wave functions. Thus, these electrons can be considered to be quasi-free in the system studied. By examining the atom-resolved DOS (Fig. 3), it becomes clear that the $E^{1/2}$ contribution to the total DOS outside the Fermi energy region is completely due to the Al states. The Fe and Ni atoms contribute to the total DOS only within the Fermi energy region, i.e., between about −4 to 2 eV. A highly peaked DOS structure occurs in this energy region. The states in this energy region are of *d* character and are characteristic of the transition metal valence states. These *d* states are highly localized in comparison to the *s* and *p* states. One can regard the electronic wave functions of the Fe and Ni *d* states to be tightly bound to their parent nuclei. Thus, these states occur in a narrow energy region.

The DOS due to the Fe states is highly peaked (Fig. 3) in the energy region between about −2.5 to 0 eV, whereas the Ni *d* states are peaked in the energy region between about −4 to −2 eV. This can be explained by the fact that for Ni, the *d*-shell is closer to being completely filled, resulting in semi core-like states. This, however, is not the case for Fe. As a result of the hybridization between the Fe and Ni *d* states and the Al 2*p* states, a deep minimum in DOS, or a pseudogap, centered at ~0.30 eV above E_F is formed. The existence of such a pseudogap at or in the vicinity of E_F is a characteristic feature of DOS of Hume-Rothery alloys containing transition metal elements [25,26,29–31]. It has also been predicted and observed in approximants to icosaherdral quasicrystals [1,26,32–34], in icosahedral quasicrystals [1,35–43], in approximants to decagonal quasicrystals [1,27,28,44,45], and in some decagonal quasicrystals [46,47].

The width of the pseudogap in $Al_{72}Ni_9Fe_{19}$ (Fig. 3) is ~0.35 eV. This pseudogap splits the band between the bonding and antibonding states. Inspection of Fig. 3 allows one to understand the nature of chemical bonds in $Al_{72}Ni_9Fe_{19}$. There is virtually no energy region in which the Ni and Fe states do not overlap with the Al

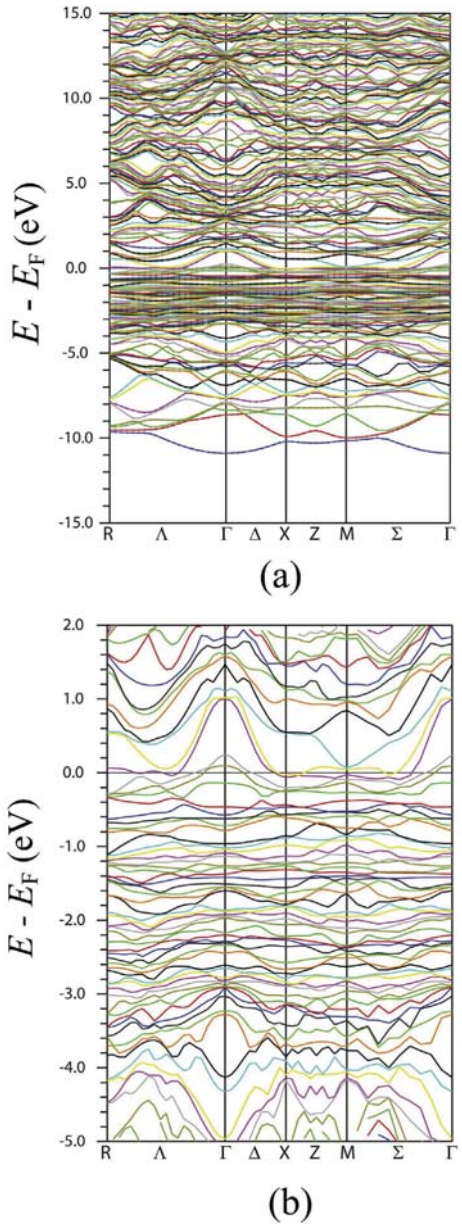

Fig. 4. Energy band structure of $Al_{72}Ni_9Fe_{19}$ for the energy range between −15 and 15 eV (a) and between −5 and 2 eV (b).

states. This shows that chemical bonds in $Al_{72}Ni_9Fe_{19}$ are covalent in nature. Moreover, the absence of energy band gaps in the Fermi energy region, indicates good metallicity of $Al_{72}Ni_9Fe_{19}$.

Fig. 4 shows the calculated electronic band structure of $Al_{72}Ni_9Fe_{19}$. One observes that the band structure is rich in numerous energy bands. The large number of bands results from a large number of atoms (28) in a unit cell (Fig. 1). A very high density of bands exists in the energy window between about −4 to 0 eV. It originates from the Fe and Ni 3*d* states. The large number of accessible states in this energy window gives rise to good metallicity of $Al_{72}Ni_9Fe_{19}$. Furthermore, these bands have very small bandwidths, which indicates their *d*-type character. Small variations in energies of these bands along various directions of the Brillouin zone are characteristic of localized states, which confirms the earlier conclusion based on the analysis of the calculated DOS.

Apart from the Fermi energy region, one encounters a relatively smaller number of bands that extend over a wide range of energies (Fig. 4). These bands appear to have larger bandwidths which indicates that they must be of *s* and *p* character. These bands are thus associated with the Al electronic states. The bands below about −5 eV originate from the strongly bound 1*s*, 2*s*, and 2*p* states, which are atomic-like states. The Al valence bands and semi-core bands are in the energy region between about −5 to 0 eV. These bands are related to the Al 3*s* and 3*p* states. Above E_F is the realm of numerous conduction bands which also originate from the unoccupied Al states. One can observe (Fig. 4) that there is no energy gap across the Fermi level, which confirms the metallic nature of the system studied.

3.2.2. Charge density distribution

The calculated electronic charge density distributions along the $z = 0.25$ plane (parallel to the *ab* plane and perpendicular to the *c*-axis) and along the $[\bar{1}20]$ direction are shown in Fig. 5. The hexagonal structure of the charge density distribution in the lattice is clearly seen (Fig. 5(a)). Equilateral triangle patterns formed by Fe/Ni atoms chemically bound to Al atoms are observed. The green regions that form the sides of the equilateral triangles indicate the presence of the directional covalent bonding between the Fe/Ni and Al atoms. There is virtually no electron charge density at the centers (red regions) of the triangles. The vertices of the triangles are the electron charge densities corresponding to Fe/Ni(1) atoms occupying the 2*d* sites (Table 1) and the charge densities between the vertices correspond to the Al(2) atoms at the 6*h* sites. Between the triangles are the regions of smaller electron charge density (yellow-orange regions). The electron charge density at the centers of these regions corresponds to the Fe/Ni(2) atoms at the 6*h* sites (Table 1). These atoms are rather isolated and the valence charge density is localized around the atomic cores.

An important factor that determines the formation of the covalent bonds and their strength is the Coulomb interaction potential between neighboring atoms. As one can observe in Fig. 5(a), atoms that are spatially close to each other are more likely to form bonds with each other. This is due to the fact that the electrostatic interaction potential varies inversely with the separation between the atoms. A large interaction potential between the positive cores of neighboring atoms and the electrons causes the electron cloud to deform its spherical shape and smear out between its parent atom and neighboring atoms in certain directions, thus forming the directional covalent bonds. Along the directions which have a smaller atomic density in a unit cell, weaker covalent bonds form. This is a result of the attractive potential of the atomic cores which is strong enough to keep the valence electron cloud in a spherical form. This is the case for the electron charge densities corresponding to the Fe/Ni(2) atoms (Fig. 5(a)).

Fig. 5(b) shows a region of two twisted, parallel electron charge density chains (layers) corresponding to the alternating Fe/Ni(1)-Al(3)-Fe/Ni(2) atoms. This region is of high electron charge density and is separated from a similar neighboring region by an area of vanishing electron charge density that is occupied by spherical high electron charge density areas due to almost isolated Al(2) atoms. Strong covalent bonds can be observed to form between Fe/Ni(1), Al(3), and Fe/Ni(2) atoms (green regions). As there are 28 atoms in a unit cell of $Al_{72}Ni_9Fe_{19}$ (Fig. 1), Al(3) and Fe/Ni(2) atoms have the highest concentration in the unit cell. Consequently, their average distances are smaller than those between Al(1), Al(2), and Fe/Ni(1) atoms. Thus, the spatial atomic distribution alone explains the observed electron charge distribution in Fig. 5.

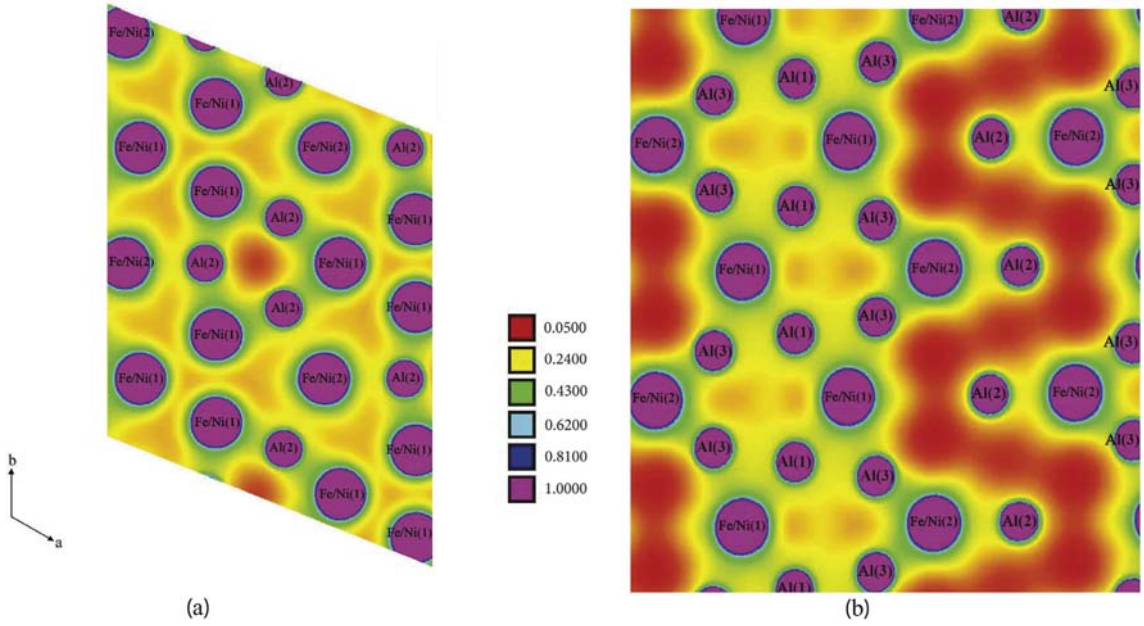

Fig. 5. Electron charge density distribution (in units of e/Å^3) along the $z = 0.25$ plane (a) and along the $[\bar{1}20]$ direction (b).

3.2.3. Hyperfine interaction parameters

Mößbauer spectra of a paramagnetic compound, or of a magnetically ordered compound at temperatures above its ordering temperature, give information on two hyperfine-interaction parameters: the quadrupole splitting (the separation between two resonance lines in a ^{57}Fe Mößbauer quadrupole doublet) $\Delta = \frac{1}{2}eQ|V_{zz}|\sqrt{1+\eta^2/3}$, where e is the proton charge, Q is the electric quadrupole moment of the ^{57}Fe nucleus (0.15 b) [48], V_{zz} is the principal component of the electric field gradient (EFG) tensor, and η is the asymmetry parameter, and the isomer shift, δ_0 [20]. For a crystalline compound of known crystal structure, V_{zz}, η, and δ_0 can be also obtained from first-principles calculations [49]. The calculated V_{zz} and η values at the two crystallographic sites occupied by Fe atoms (and also at three crystallographic sites occupied by Al atoms - these might be of relevance for future ^{27}Al nuclear magnetic resonance experiments), are displayed in Table 1 and their comparison with experiment will be discussed below.

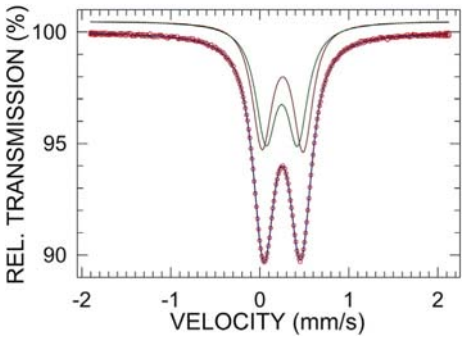

Fig. 7. ^{57}Fe Mößbauer spectrum of $Al_{72}Ni_9Fe_{19}$ at 295.5 K fitted (blue solid line) with two quadrupole doublets corresponding to the Fe atoms at the Fe(1) site (dark green solid line) and at the Fe(2) site (dark red solid line). The zero-velocity origin is relative to α-Fe at room temperature. (For interpretation of the references to colour in this figure legend, the reader is referred to the web version of this article.)

3.3. Mößbauer spectroscopy

In order to access the possibility of the presence of an Fe-containing impurity phase in the sample studied, we measured the room- and liquid-nitrogen temperature ^{57}Fe Mößbauer spectra of $Al_{72}Ni_9Fe_{19}$ over a large velocity range (Fig. 6). Apart from a quadrupole doublet originating from the main phase, that results from a superposition of two quadrupole doublets corresponding to the Fe atoms at the 2*d* and 6*h* sites (*vide infra*), no Zeeman pattern or additional quadrupole doublet originating from a possible magnetic/nonmagnetic impurity phase present in the studied specimen can be discerned in the spectra (Fig. 6). Thus, if the compound studied does contain an Fe-based magnetic or nonmagnetic impurity phase, its amount must be below the ^{57}Fe Mößbauer spectroscopy detection limit.

Fig. 7 displays the room-temperature Mößbauer spectrum of $Al_{72}Ni_9Fe_{19}$. Although the experimental spectrum is in a form of a structureless quadrupole doublet, one cannot obtain a satisfactory fit with one quadrupole doublet component. Two quadrupole doublet components of the same spectral area result in a very good fit (Fig. 7). This is in agreement with the fact that the Fe atoms are located at two inequivalent crystallographic sites (Table 1). The quadrupole doublet component with a smaller Δ is assigned to the Fe(1) atoms (at the 2*d* sites) and that with a larger Δ is assigned to the Fe(2) atoms (at the 6*h* sites). This assignment is based on the calculated values of Δ (using the calculated values of V_{zz} and η from Table 1) that are 0.343 and 0.516 mm/s at the 2*d* and 6*h* sites, respectively.

The Mößbauer spectra of $Al_{72}Ni_9Fe_{19}$ at various temperatures

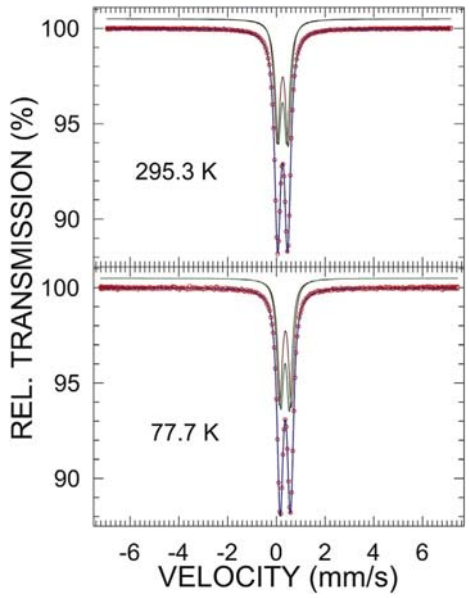

Fig. 6. Room- and liquid-nitrogen temperature ^{57}Fe Mößbauer spectra of $Al_{72}Ni_9Fe_{19}$ measured in a large velocity range fitted (blue solid line) with two quadrupole doublets (dark green and dark red solid lines), as described in the text. The zero-velocity origin is relative to α-Fe at room temperature. (For interpretation of the references to colour in this figure legend, the reader is referred to the web version of this article.)

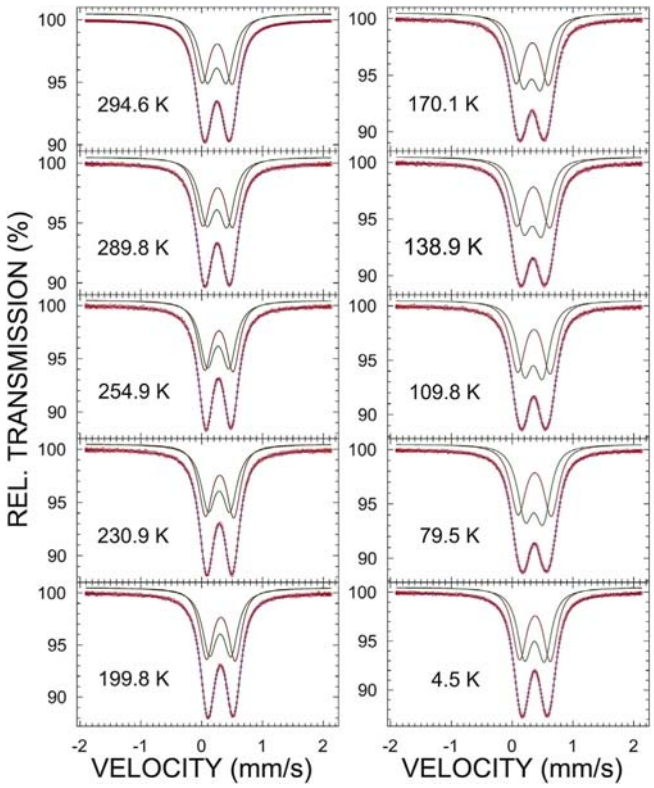

Fig. 8. ^{57}Fe Mößbauer spectra of $Al_{72}Ni_9Fe_{19}$ at the indicated temperatures fitted (blue solid lines) with two quadrupole doublets corresponding to the Fe atoms at the Fe(1) site (dark green solid lines) and at the Fe(2) site (dark red solid lines). The zero-velocity origin is relative to α-Fe at room temperature. (For interpretation of the references to colour in this figure legend, the reader is referred to the web version of this article.)

down to 4.5 K are shown in Fig. 8. Their shape is exactly the same as that of the spectrum in Fig. 7. The best fits of these spectra could then be obtained with two quadrupole doublet components corresponding to the Fe atoms at the Fe(1) and Fe(2) sites. The persistence of a quadrupole doublet spectrum down to 4.5 K proves the alloy studied does not order magnetically down to 4.5 K, i.e., that this alloy is a paramagnet.

Fig. 9 shows the temperature dependence of Δ_i (i = 1,2) obtained from the fits of the spectra in Figs. 7 and 8. One can notice that the values of Δ_1 and Δ_2 are approximately constant at temperatures above ~200 K and then decrease/increase at lower temperatures. A sudden decrease(increase) of $\Delta_1(\Delta_2)$ below ~200 K could be caused by a possible structural phase transition at ~200 K. One also observes that the low-temperature values of Δ_1 and Δ_2 are in a very good agreement with the corresponding calculated values of 0.343 and 0.516 mm/s.

The temperature dependence of the centre shifts $\delta_i(T)$ (i = 1,2) corresponding to the two component quadrupole doublets, that was determined from the fits of the spectra in Figs. 7 and 8, is shown in Fig. 10. The centre shift at temperature T, $\delta(T)$, consists of two contributions

$$\delta(T) = \delta_0 + \delta_{SOD}(T), \quad (1)$$

where δ_0 is the intrinsic, temperature-independent isomer shift and $\delta_{SOD}(T)$ is the second-order Doppler (SOD) shift which depends on the lattice vibrations of the Fe atoms [20]. The latter contribution can be expressed in terms of the Debye approximation of the lattice vibrations as

$$\delta_{SOD}(T) = -\frac{9}{2}\frac{k_B T}{Mc}\left(\frac{T}{\Theta_D}\right)^3 \int_0^{\Theta_D/T} \frac{x^3 dx}{e^x - 1}, \quad (2)$$

where k_B is the Boltzmann constant, M is the mass of the Mößbauer nucleus, c is the speed of light, and Θ_D is the Debye temperature. The fits of the experimental data $\delta_i(T)$ (Fig. 10) to Eq. (1) yield the quantities $\delta_{0,i}$ and $\Theta_{D,i}$: $\delta_{0,1} = 0.367(1)$ mm/s, $\Theta_{D,1} = 433(4)$ K, and $\delta_{0,2} = 0.375(1)$ mm/s,$\Theta_{D,2} = 428(5)$ K. The weighted average of Θ_D is then 431 (3) K. This value of Θ_D is exactly the same as that found for another approximant to a decagonal Al-Ni-Fe quasicrystal, $Al_{76}Ni_9Fe_{15}$ [28].

3.4. Magnetic measurements

Although Mößbauer spectra in Figs. 6–8 indicate the absence of a possible magnetic impurity in the specimen studied, the magnetic field dependence of magnetization curves $M(H)$ measured at selected temperatures (Fig. 11) are typical of a ferromagnet. These curves do not saturate in the highest field available of 90 kOe. It is concluded that the specimen studied contains a ferromagnetic impurity (at the ppm concentration level), probably in the form of an iron-oxide phase at the sample's surfaces or precipitated iron superparamagnetic clusters.

The temperature dependence of the magnetic susceptibility χ of $Al_{72}Ni_9Fe_{19}$ measured in an applied magnetic field of 10 kOe is shown in Fig. 12. It follows approximately a $1/T$-like dependence characteristic of the Curie-Weiss law. In order to account for the presence in the specimen studied of a small amount of ferromagnetic impurity with the saturation magnetization M_0, the $\chi(T)$ data were fitted to the equation containing an additional $T^{3/2}$ term associated with Bloch spin-waves [50,51]

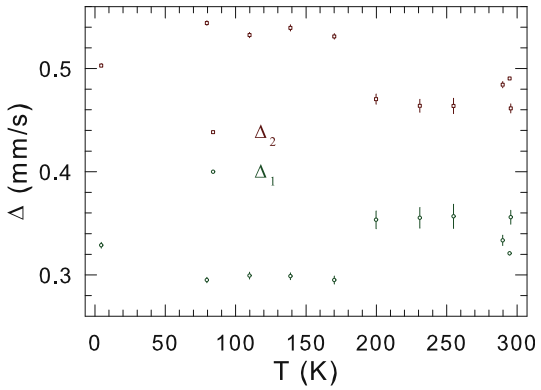

Fig. 9. Temperature dependence of the quadrupole splittings $\Delta_i(T)$ (i = 1,2) of Fe at the Fe(1) and Fe(2) sites (Table 1).

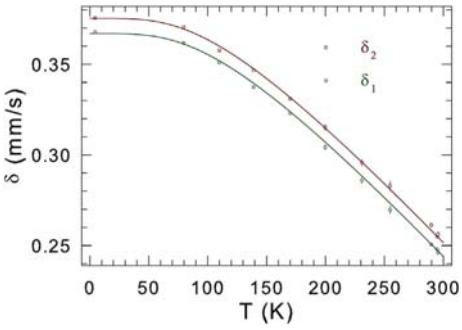

Fig. 10. Temperature dependence of the centre shifts $\delta_i(T)$ (i = 1,2) of the Fe(1)- and Fe(2)-site quadrupole doublets. The solid lines are the fits to Eq. (1), as explained in the text.

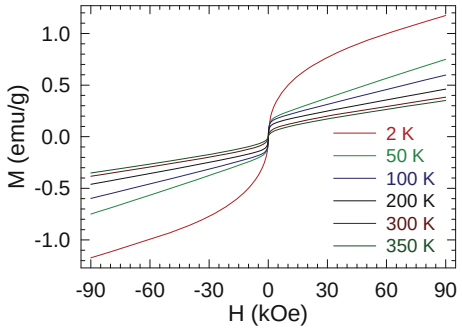

Fig. 11. Hysteresis curves of $Al_{72}Ni_9Fe_{19}$ at selected temperatures in the magnetic field range −90 – +90 kOe.

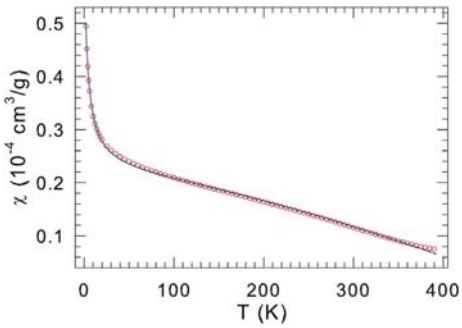

Fig. 12. Temperature dependence of the magnetic susceptibility of $Al_{72}Ni_9Fe_{19}$ measured in an external magnetic field of 10 kOe. The solid line is the fit to Eq. (3), as explained in the text.

$$\chi = \chi_0 + \frac{C}{T-\Theta_p} + \frac{M_0}{H}\left(1 - a_{3/2}T^{3/2}\right), \quad (3)$$

where χ_0 is the temperature-independent term that includes contributions from Pauli and Van Vleck paramagnetism as well as core and Landau diamagnetism, C is the Curie constant, and Θ_p is the paramagnetic Curie temperature. The Curie constant can be expressed as $C = \frac{N\mu_{eff}^2}{3k_B}$, where N is the number of transition metal (TM) atoms per formula unit and μ_{eff} is the effective magnetic moment. The value of $M_0 = 0.617$ emu/g used in the fit was estimated from a linear extrapolation of the 2 K $M(H)$ curve (Fig. 11) to $H = 0$. The fit of the $\chi(T)$ data (Fig. 12) to Eq. (3) gives $\chi_0 = 1.44(1) \times 10^{-5}$ cm^3/g, $C = 1.59(3) \times 10^{-4}$ cm^3 K/g, and $\Theta_p = -3.71(13)$ K. The negative value of Θ_p indicates the antiferromagnetic interaction between the TM atoms. The value of C corresponds to $\mu_{eff} = 0.401(4)\ \mu_B$ per TM atom.

4. Summary

The results of *ab-initio* electronic structure and electric field gradient calculations, and of X-ray diffraction, ^{57}Fe Mößbauer spectroscopy, and magnetic measurements of the approximant $Al_{72}Ni_9Fe_{19}$ to a decagonal Al-Ni-Fe quasicrystal are presented. The compound studied crystallizes in the hexagonal space group $P6_3/mmc$ with the lattice parameters $a = 7.6989(2)$ Å and $c = 7.6724(2)$ Å. The existence of a pseudogap is observed in the calculated DOS, that is centered at ~0.30 eV above the Fermi level and with a width of ~0.35 eV. Good metallicity of $Al_{72}Ni_9Fe_{19}$ is predicted and covalent nature of the chemical bonding is evidenced. The approximant studied is shown to be a paramagnet down to 2.0 K. The Mößbauer spectra are shown to result from a superposition of two quadrupole doublets originating from Fe atoms located at two inequivalent crystallographic sites. A possible structural transition is inferred from a sudden change of the quadrupole splittings of the two doublets at ~200 K. Good agreement is observed between the calculated and measured quadruopole splittings. It is found that the Debye temperature of $Al_{72}Ni_9Fe_{19}$ is 431 (3) K.

Acknowledgements

This work was supported by the Natural Sciences and Engineering Research Council of Canada.

References

[1] Z.M. Stadnik (Ed.), Physical Properties of Quasicrystals, Springer-Verlag, Berlin, 1999;
[a] J.-B. Suck, M. Schreiber, P. Häussler (Eds.), Quasicrystals, an Introductions to Structure, Physical Properties, and Applications, Springer-Verlag, Berlin, 2002;
[b] T. Fujiwara, Y. Ishii (Eds.), Quasicrystals, Elsevier, Amsterdam, 2008.
[2] A.P. Tsai, J.Q. Guo, E. Abe, H. Takakura, T.J. Sato, Nature 408 (2000) 538.
[3] P. Wang, Z.M. Stadnik, K. Al-Qadi, J. Przewoźnik, J. Phys. Condens. Matter 21 (2009) 436007.
[4] V. Elser, C.L. Henley, Phys. Rev. Lett. 55 (1985) 2883.
[5] A.I. Goldman, K.F. Kelton, Rev. Mod. Phys. 65 (1993) 213.
[6] Z.M. Stadnik, in: K.H.J. Buschow (Ed.), Handbook of Magnetic Materials, vol. 21, Elsevier, Amsterdam, 2013, p. 77.
[7] S. Song, E.R. Ryba, Philos. Mag. Lett. 65 (1992) 85.
[8] J.B. Newkirk, P.J. Black, A. Damjanovic, Acta Cryst. 14 (1961) 532.
[9] U. Burkhardt, M. Ellner, Yu Grin, B. Baumgartner, Power Diffr. 13 (1998) 159.
[10] K. Yamamoto, M. Jono, Y. Matsuo, J. Phys. Condens. Matter 11 (1999) 1015.
[11] G. Trambly de Laissardière, D.N. Manh, L. Magaud, J.P. Julien, F. Cyrot-Lackmann, D. Mayou, Phys. Rev. B 52 (1995) 7920.
[12] E. Belin-Ferré, G. Trambly de Laissardière, P. Pecheur, A. Sadoc, J.M. Dubois, J. Phys. Condens. Matter 9 (1997) 9585.
[13] G. Trambly de Laissardière, Phys. Rev. B 68 (2003) 045117.
[14] A. Ormeci, Y. Grin, Isr. J. Chem. 51 (2011) 1349.
[15] A.J. Bradley, A. Taylor, Proc. R. Soc. Lond. Ser. A 166 (1938) 353.
[16] I. Chumak, K.W. Richter, H. Ipser, Intermetallics 15 (2007) 1416.
[17] P. Blaha, K. Schwartz, G. Madsen, D. Kvasnicka, J. Luitz, in: Karlheinz Schwarz (Ed.), WIEN2k, an Augmented Plane Wave Plus Local Orbitals Program for Calculating Crystal Properties, Technical Universität Wien, Austria, 1999.
[18] J.P. Perdew, S. Burke, M. Ernzerhof, Phys. Rev. Lett. 77 (1996) 3865.
[19] B. Grushko, U. Lemmerz, K. Fisher, C. Freiburg, Phys. Stat. Sol. A 155 (1996) 17.
[20] N.N. Greenwood, T.C. Gibb, Mössbauer Spectroscopy, Chapman and Hall, London, 1971;
[a] P. Gütlich, E. Bill, A. Trautwein, Mössbauer Spectroscopy and Transition Metal Chemistry, Springer, Berlin, 2011.
[21] Natl. Bur. Stand. (U.S.) Circ. No. 1541J.P. Cali (Ed.), Certificate of Calibration, Iron Foil Mössbauer Standard, U.S. GPO, Washington, D.C., 1971.
[22] S. Margulies, J.R. Ehrman, Nucl. Instrum. Methods 12 (1961) 131;
[a] G.K. Shenoy, J.M. Friedt, H. Maletta, S.L. Ruby, in: I.J. Gruverman, C.W. Seidel, D.K. Dieterly (Eds.), Mössbauer Effect Methodology, vol. 10, Plenum, New York, 1974, p. 277.
[23] R.A. Young, The Rietveld Method, Oxford University Press, Oxford, 1993.
[24] N.W. Ashcroft, N.D. Mermin, Solid State Physics, Holt, Rinehart and Winston, Philadelphia, PA, 1976.
[25] G. Trambly de Laissardière, D. Nguyen-Manh, L. Magaud, J.P. Julien, F. Cyrot-Lackmann, D. Mayou, Phys. Rev. B 52 (1995) 7920.
[26] G. Trambly de Laissardière, D. Nguyen-Manh, D. Mayou, Prog. Mater. Sci. 50 (2005) 679.
[27] M.A. Albedah, F. Nejadsattari, Z.M. Stadnik, J. Przewoźnik, J. Alloy. Compd. 619 (2015) 839.
[28] F. Nejadsattari, Z.M. Stadnik, J. Przewoźnik, B. Grushko, J. Alloy. Compd. 662 (2016) 612.
[29] R. Asahi, H. Sato, T. Takeuchi, U. Mizutani, Phys. Rev. B 71 (2005) 165103.
[30] R. Asahi, H. Sato, T. Takeuchi, U. Mizutani, Phys. Rev. B 72 (2005) 125102.
[31] U. Mizutani, R. Asahi, H. Sato, T. Takeuchi, Phys. Rev. B 74 (2006) 235119.
[32] H. Sato, T. Takeuchi, U. Mizutani, Phys. Rev. B 64 (2001) 094207.
[33] T. Takeuchi, T. Onogi, T. Otagiri, U. Mizutani, H. Sato, K. Kato, T. Kamiyama, Phys. Rev. B 68 (2003) 184203.
[34] H. Sato, T. Takeuchi, U. Mizutani, Phys. Rev. B 70 (2004) 024210.
[35] Z.M. Stadnik, D. Purdie, M. Garnier, Y. Bauer, A.-P. Tsai, A. Inoue, K. Edagawa, S. Takeuchi, Phys. Rev. Lett. 77 (1996) 1777.
[36] Z.M. Stadnik, D. Purdie, M. Garnier, Y. Bauer, A.-P. Tsai, A. Inoue, K. Edagawa, S. Takeuchi, K.H.J. Buschow, Phys. Rev. B 55 (1997) 10938.
[37] Z.M. Stadnik, D. Purdie, T.A. Lograsso, Phys. Rev. B 64 (2001) 214202.
[38] Z.M. Stadnik, Mater. Trans. JIM 42 (2001) 920.
[39] R. Tamura, Y. Murao, S. Takeuchi, T. Kiss, T. Yokoya, S. Shin, Phys. Rev. B 65 (2002) 224202.
[40] A. Suchodolskis, W. Assmus, L. Giovanelli, U.O. Karlsson, V. Karpus, G. Le Lay, E. Sterzel, E. Uhrig, Phys. Rev. B 68 (2003) 054207.
[41] R. Widmer, P. Gröning, M. Feuerbacher, O. Gröning, Phys. Rev. B 79 (2009) 104202.
[42] H.R. Sharma, G. Simutis, V.R. Dhanak, P.J. Nugent, C. Cui, M. Shimoda, R. McGrath, A.P. Tsai, Y. Ishii, Phys. Rev. B 81 (2010) 104205.
[43] J. Nayak, M. Maniraj, A. Gloskovskii, M. Krajčí, S. Sebastian, I.R. Fisher, K. Horn, S.R. Barman, Phys. Rev. B 91 (2015) 235116.
[44] M. Krajčí, J. Hafner, M. Mihalkovič, Phys. Rev. B 73 (2006) 134203.
[45] K.H. Hassdenteufel, A.R. Oganov, S. Katrych, W. Steurer, Phys. Rev. B 75 (2007) 144115.
[46] T. Suzuki, H.R. Sharma, T. Nishimura, M. Shimoda, Y. Yamauchi, A.-P. Tsai, Phys. Rev. B 72 (2005) 115427.
[47] T. Mertelj, A. Oštlak, J. Dolinšek, I.R. Fisher, V.V. Kabanov, D. Mihailovic, Phys. Rev. Lett. 102 (2009) 086405.
[48] G. Martínez-Pinedo, P. Schwerdtfeger, E. Caurier, K. Langanke, W. Nazarewich, T. Söhnel, Phys. Rev. Lett. 87 (2001) 062701.
[49] P. Blaha, J. Phys. Conf. Ser. 217 (2010) 012009.
[50] F. Müller, M. Rosenberg, W. Liu, U. Köster, Mater. Sci. Eng. A 134 (1991) 900.
[51] Z.M. Stadnik, F. Müller, Philos. Mag. B 71 (1995) 221.